Materials and Design 30 (2009) 1966–1975

Contents lists available at ScienceDirect

Materials and Design

journal homepage: www.elsevier.com/locate/matdes

Titanium alloy lattice truss structures

Douglas T. Queheillalt *, Haydn N.G. Wadley

Department of Materials Science and Engineering, University of Virginia, 140 Chemistry Way, P.O. Box 400745, Charlottesville, VA 22904-4745, United States

ARTICLE INFO

Article history:
Received 21 March 2007
Accepted 3 September 2008
Available online 20 September 2008

Keywords:
Sandwich structures (B)
Diffusion bonding (D)
Buckling (I)

ABSTRACT

A high-temperature forming and diffusion bonding method has been investigated for the fabrication of modified pyramidal lattice core sandwich structures from a titanium alloy. A periodic asymmetric hexagonal perforation pattern was cut into thin Ti–6Al–4V sheets which were then folded along node rows by a combination of partial low-temperature bending followed by simultaneous hot forming/diffusion bonding to form sandwich panel structures with core relative densities of 1.0–4.1%. The out-of-plane compression and in-plane longitudinal shear properties of these structures were measured and compared with analytical estimates. Premature panel failure by node shear-off fracture was observed during shear testing of some test structures. Node failures were also initiated at stress concentrations at the truss–facesheet interface. A liquid interface diffusion bonding approach has been investigated as a possible approach for reducing this stress concentration and increasing the truss–facesheet interfacial strength.

Published by Elsevier Ltd.

1. Introduction

Lightweight metallic sandwich panel structures consisting of low density cores and solid facesheets are widely used in aerospace applications [1–5]. Cellular core structures based upon honeycomb topologies are most often used because of their high compressive and flexural stiffness and strength-to-weight ratios, good vibration damping and low through thickness thermal conductivity [6–8]. These honeycomb structures are closed-celled with no access to the core region and are susceptible to internal corrosion [6]. Lattice truss structures with tetrahedral, pyramidal and Kagomé cell topologies are beginning to be explored as alternate core materials. For example, pyramidal lattice truss structures can be fabricated from ductile aluminum and stainless steel alloys by perforating a metal sheet to form a periodic diamond perforation pattern, followed by a node row folding process [9–14]. The folded core can be brazed or laser welded to solid facesheets to form a sandwich structure. The lattice topology, core relative density and parent alloy mechanical properties combine to determine the mode of truss deformation and therefore the mechanical response of these structures [9,10].

Previous studies with lattices fabricated from high elastic modulus, low strength stainless steels indicate that high core relative density cores fail by yielding of the truss columns [9–11,13,14]. For elastic–perfectly plastic materials, the peak out-of-plane compressive strength, σ_{pk}, scales linearly with the relative density; $\sigma_{pk} = \Sigma\sigma_{ys}\bar{\rho}$ where Σ is a lattice topology (geometry) dependent scaling factor (for a pyramidal lattice, $\Sigma = \sin^2\omega$, where ω is the angle of inclination of the truss), σ_{ys} is the yield strength of the solid material and the relative density $\bar{\rho} = \rho_c/\rho_s$ is the density of the core, ρ_c, divided by that of the solid material, ρ_s. Increasing the solid materials yield strength enables the lattice strength to be increased when yielding is the operative failure mode. Table 1 summarizes the specific yield strength for several alloys that have been used to fabricate lattice truss structures. Data for Ti–6Al–4V is also shown. It has the highest specific yield strength and a significantly higher maximum service temperature than 6061 aluminum alloys. A lattice structure fabricated from Ti–6Al–4V might therefore have useful applications.

Here, we explore the use of a modified form of the sheet folding method, developed for highly ductile materials, and used it to fabricate modified pyramidal lattice structures from a Ti–6Al–4V alloy. A combination of cold and hot forming/diffusion bonding was needed to fabricate the sandwich panel structures. The out-of-plane compressive and in-plane longitudinal shear properties have been measured and compared with analytical estimates for truss plastic yielding and buckling. The resulting structures have higher strength-to-weight ratios than similar lattices made from either heat treatable aluminum or stainless steel alloys. Premature panel failure by node flat shear fracture and node truss shear-off fracture was observed during shear testing of some structures. A liquid interface diffusion bonding technique was investigated as a possible approach for the mitigation of this failure mode.

2. Fabrication approach

2.1. Forming limit considerations

Pyramidal lattice structures can be fabricated from high ductility materials by a folding process [10–13]. However, when this was

* Corresponding author. Tel.: +1 434 982 5678; fax: +1 434 982 5677.
E-mail address: dougq@virginia.edu (D.T. Queheillalt).

0261-3069/$ - see front matter Published by Elsevier Ltd.
doi:10.1016/j.matdes.2008.09.015

Table 1
Selected mechanical and physical properties of various alloys used for fabrication of lattice truss sandwich structures

Material	Yield strength, σ_y (MPa)	Density, ρ_s (kg/m^3)	Maximum use temperature, T (°C)	$\times 10^3$ σ_y/ρ_s
Al 6061-H0	70	2700	~170	26
Al 6061-T6	268	2700	~170	99
304 SS	176	8000	~925	22
Al6XN SS	200	8000	~420	25
Ti–6Al–4V	900	4430	~420	203

attempted here the limited ambient temperature formability of Ti–6Al–4V resulted in sheet fracture on the tensile stress side of the node after only a half of the required bending deflection. This problem is commonly encountered during deformation processes with low ductility alloys [15,16]. The minimum bend radius (the radius at which cracks appear on the tensile stressed surface of a bend) for sheet material under plane strain conditions has been analyzed by Yang [17]. He shows that the minimum bend radius, R, depends on the sheet thickness, t, and tensile ductility, e_t:

$$R = t\left(\frac{50}{e_t} - \frac{1}{2}\right) \quad (1)$$

where e_t is the tensile elongation to failure of the solid material in% and is expressed as a function of sheet thickness [17].

Fig. 1 shows the minimum bend radius/sheet thickness ratio predicted by Eq. (1). Typical ambient temperature tensile ductility ranges for various alloys are overlaid [18,19]. Fabrication of pyramidal lattice structures via a folding process that bends a diamond perforated sheet with a point node to create a single layer of trusses is facilitated by R/t values $\leqslant$1.5. This requires a minimum tensile elongation of about 25%. Titanium alloys have tensile elongations in the 10–15% range. The corresponding bend radius to thickness ratio then lies in the range $2.5 \leqslant R/t \leqslant 4$ which precludes the fabrication of pyramidal lattices by an ambient temperature bend forming approach.

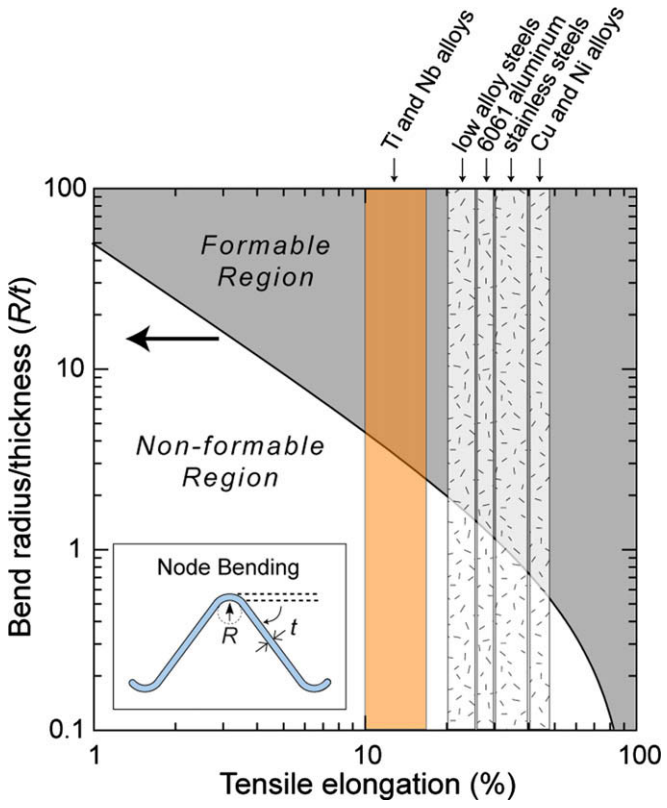

Fig. 1. The minimum bend radius/sheet thickness ratio as a function of tensile elongation for various alloys (all data is for alloys in the fully annealed condition at ambient temperature). As the alloy ductility decreases it becomes much more difficult to form lattice truss structures by bending.

To accommodate the lower ductility of this alloy, the fabrication process was modified in two ways. The pyramidal lattice itself was first modified to create a unit cell structure with a short flat nodal region. Fig. 2a and b shows schematic illustrations of an ideal and the modified unit cell geometries, respectively. This flat nodal region then enables the use of a larger bending radius folding operation. It also has the beneficial consequences of increasing the node contact area and thus the fracture strength of the node. However, this is accompanied by a reduction of structural efficiency (by the ratio of the mass of material utilized in the node to the total core mass) [12]. The core was partially formed at ambient temperature and the folding was completed at the higher temperature used for diffusion bonding the core to solid facesheets.

2.2. Panel fabrication

The process consisted of perforating a metal sheet to create a modified two-dimensional periodic diamond perforation pattern, partially folding node rows by a cold bending process and then hot forming/diffusion bonding the pyramidal lattice to facesheets to form the sandwich structures. The periodic truncated-diamond pattern punched into sheets of Ti–6Al–4V is shown in Fig. 3a. An example of a partially formed modified pyramidal lattice is shown in Fig. 3b. The lattice was bent using a bend radius/thickness ratio of $R/t \sim 3$, which was sufficient to prevent cracking on the tensile side of the bend region. A close-up of the node region is shown as an inset of Fig. 3b. This bent radius region is flattened during the subsequent high-temperature forming/diffusion bonding process, Fig. 2b.

Fig. 4 shows a schematic illustration of the tool assembly for hot forming/diffusion bonding the modified pyramidal sandwich structures to solid facesheets. The room temperature formed cores were placed on tool steel load supporting pins, a bottom Ti–6Al–4V facesheet and tool steel support plate combination, Fig. 4a. A second set of tool steel load supporting pins, a top Ti–6Al–4V facesheet and tool steel support plate combination, Fig. 4b and c, was placed on top of the core forming the stacked assembly. Three of these assemblies were stacked vertically and placed in a diffusion bonding furnace. The node support pins and plates were also cleaned prior to assembly and a light coating of boron nitride applied to act as a release agent between the fixture and sandwich structures. Fig. 4d shows a schematic illustration of the hot formed/diffusion bonded cores.

For the hot forming/diffusion bonding step, the chamber was evacuated to $\sim 10^{-4}$ Torr and the stacked assembly was heated at 10 °C/min to 900 °C, held for 6 h with a pressure of 3.5 MPa applied to the assembly and finally cooled at 10 °C/min. After diffusion bonding, the node support pins were removed and compression and shear samples were wire electro-discharge machined from the sandwich panels. Fig. 5 shows photographs of typical node regions for the four relative densities investigated here.

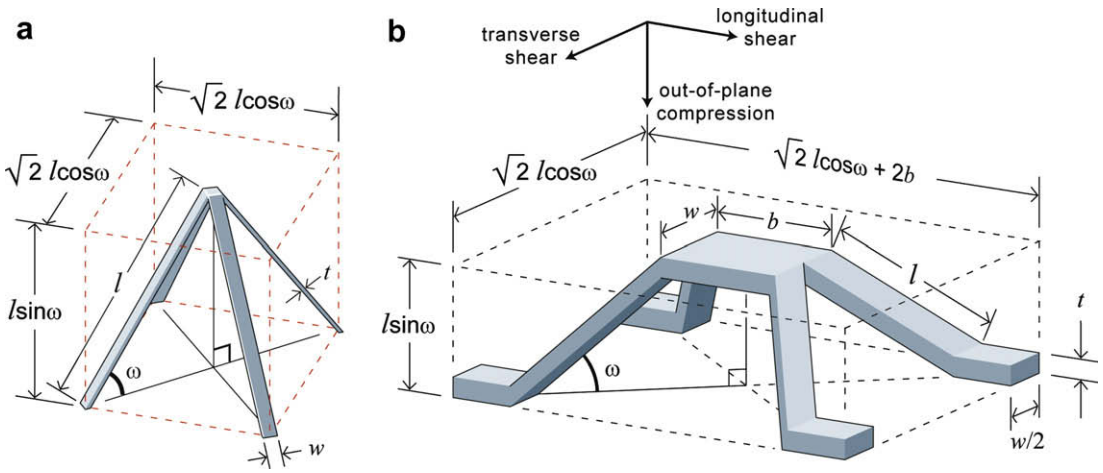

Fig. 2. Schematic illustration of (a) an ideal and (b) the modified pyramidal unit cells.

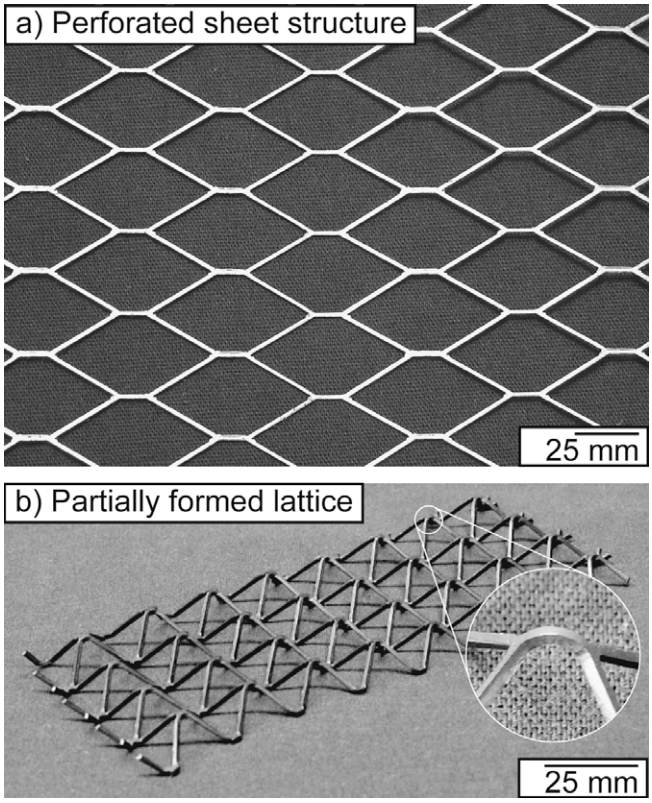

Fig. 3. Photographs of (a) the periodic asymmetric hexagonal perforation pattern applied to sheets of a Ti–6Al–4V alloy and (b) the partially formed modified pyramidal lattice.

2.3. Relative density

The modified pyramidal lattice fabricated here is similar to that made by using expanded aluminum sheets [12]. The relative density, $\bar{\rho}$, is the volume fraction of the unit cell occupied by metal. For a unit cell defined by the included truss angle, ω

$$\bar{\rho} = \frac{(2l+b)}{\sin\omega\cdot\cos\omega\cdot(l\cos\omega+\sqrt{2}b)}\left(\frac{wt}{l^2}\right), \tag{2}$$

where l is the truss member length, b is the length of a node, w and t are the width and thickness of the truss member. If $\omega = 45^\circ$ and $w = t$ (the case here), Eq. (2) reduces to

$$\bar{\rho} = 2\sqrt{2}\frac{(2l+b)}{(l+b)}\left(\frac{t}{l}\right)^2. \tag{3}$$

Samples were fabricated from sheet with thicknesses $t = 0.635$, 0.813, 1.016, 1.270 mm. A nominal truss length of $l = 10.0$ mm and a flat nodal region $b = 6.2$ mm was used for all samples. Table 2 shows a comparison between the predicted and measured relative densities for three panels at each relative density. The measured relative densities, calculated by measuring the mass of the sandwich panel minus the mass of the facesheets, are reasonably predicted and lie just below that calculated by Eq. (3). The deviation between measured and calculated relative densities is attributed to manufacturing variations which included small variations in the truss inclination angle, the finite bend radius at the nodes which was not accounted for in the theoretical calculations and variations in the core thickness over the length of the panels. There were slight variations in the measured core thickness, due to manufacturing defects, and an average core thickness was used for the measured relative density calculations.

3. Mechanical property predictions

Deshpande and Fleck [9] have developed approximate analytical expressions for the stiffness and strength of pyramidal lattice truss cores assuming elastic–plastic struts. It was assumed that the truss cores were sandwiched between rigid facesheets and their struts were of sufficiently low aspect ratio, t/l, that there bending stiffness and strength were negligible compared to their stretching stiffness and strength [9]. The collapse strength of a lattice truss core is determined by the mechanism of strut failure which depends on the cell geometry, strut material properties and the mode of failure during loading (plastic yielding and elastic or plastic buckling). The flat node region in the modified pyramidal truss structure provides no contribution to the compressive stiffness and strength or to the shear stiffness. However, it does contribute to the shear strength by providing a larger contact area between the core and facesheet. Kooistra and Wadley [12] introduced a truss mass fraction to account for the mass of material occupied by the nodes for similar lattices fabricated from an expanded aluminum alloy. Here, we have used a similar analysis and the resulting truss mass fraction for these structures is $\eta = 2l/(2l+b)$ where b is defined in Fig. 2b As b approaches zero, $\eta = 1$ (an ideal lattice). For non-ideal lattices, η is an analytical estimate of the knock-down in the stiffness and strength properties. For all of the samples tested, $\eta = 0.763$. Table 3 shows the analytical

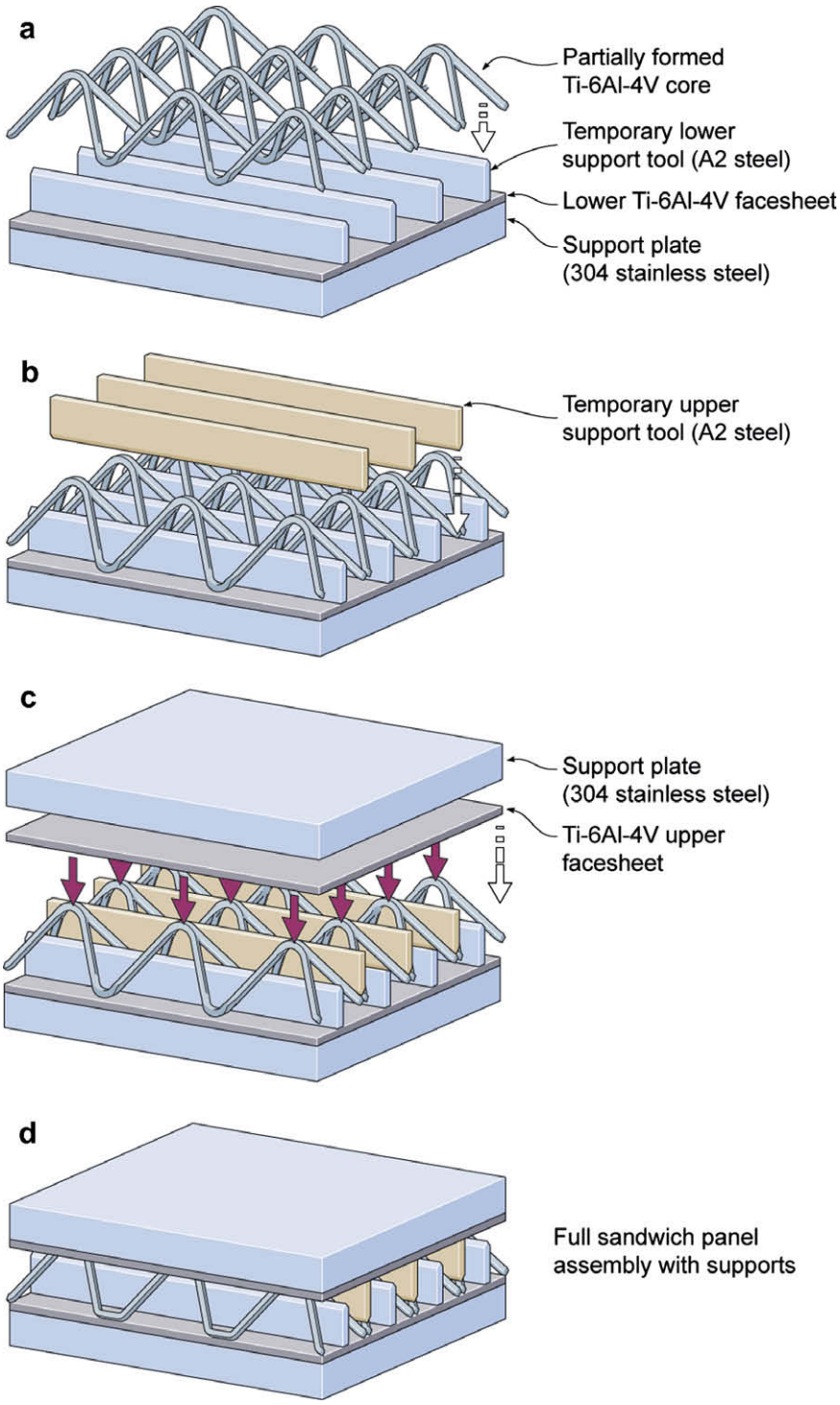

Fig. 4. Schematic illustration of the lattice structure, face sheet and tool assembly used for hot forming and diffusion bonding the modified pyramidal lattice sandwich structures.

expressions for the compressive and shear stiffness and strength of the modified pyramidal lattice truss sandwich structures.

4. Experimental mechanical response

The lattice truss structures were tested at ambient temperature in compression and shear at a nominal strain rate of $4 \times 10^{-2}\ s^{-1}$ in accordance with ASTM C365 and C273, respectively. A laser extensometer measured the facesheet displacement with a precision of ±0.001 mm. The nominal compressive strain was obtained by monitoring the displacements of the unconstrained facesheets and the nominal shear strain from the displacements of the shear fixtures. For the shear experiments, the samples were rigidly attached to the shear fixtures by steel machine screws and a leading edge stop.

To determine parent alloy properties in the diffusion bonded condition, tensile tests were performed on Ti–6Al–4V samples subjected to the same thermal cycle used for fabrication of the diffusion bonded sandwich structures. The parent material was adequately approximated as an elastic–plastic solid with Young's

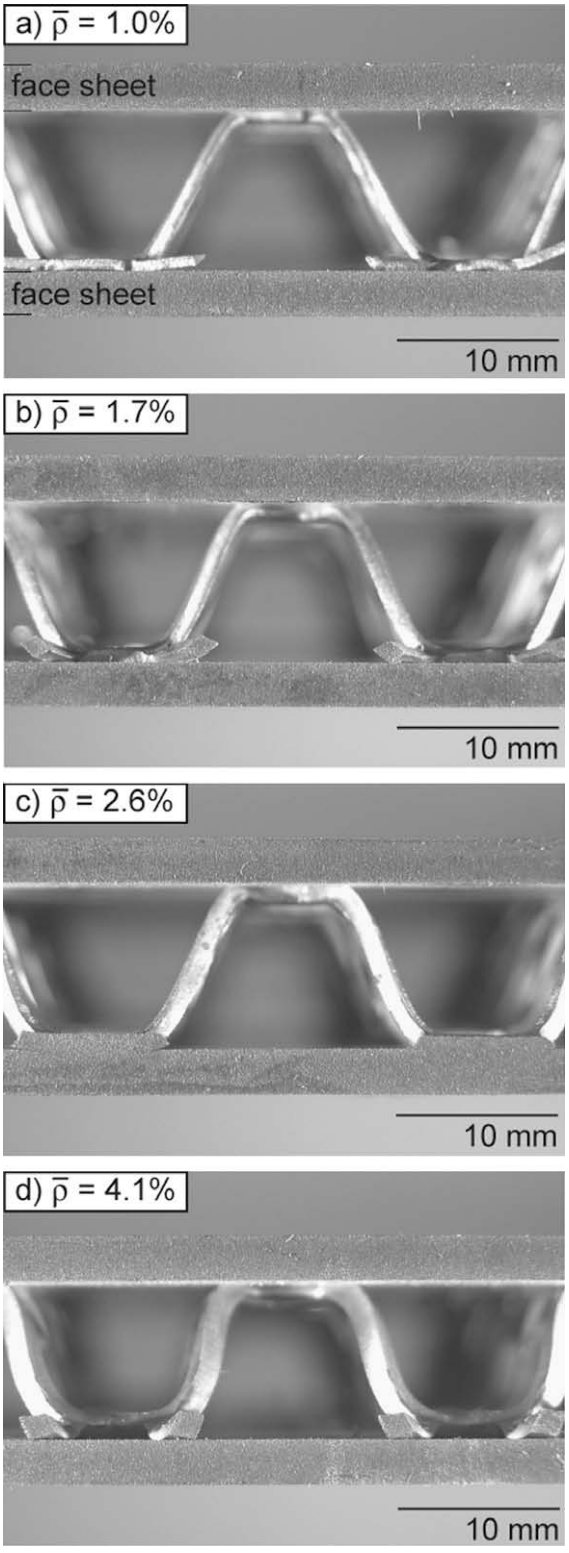

Fig. 5. Photographs of the Ti–6Al–4V modified pyramidal lattice truss structures along with their corresponding relative densities, $\bar{\rho} = 1.0\%, 1.7\%, 2.6\%, 4.1\%$.

modulus $E_s = 116$ GPa, 0.2% offset yield strength $\sigma_{ys} = 900$ MPa and a linear hardening modulus $E_t \equiv d\sigma/d\varepsilon = 1667$ MPa .

4.1. Out-of-plane compression

The through thickness compressive stress–strain responses for the Ti–6Al–4V lattice truss structures are shown in Fig. 6. Follow-

Table 2
Measured and predicted relative densities for the Ti–6Al–4V modified pyramidal lattice truss structures

Measure relative density, $\bar{\rho}$	Average relative density, $\bar{\rho}$	Predicted relative density, $\bar{\rho}$
0.0071	0.0075 ± 0.0004	0.0102
0.0079		
0.0075		
0.0139	0.0139 ± 0.0012	0.0167
0.0150		
0.0127		
0.0260	0.0259 ± 0.0003	0.0261
0.0261		
0.0256		
0.0387	0.0367 ± 0.0018	0.0407
0.0358		
0.0355		

Table 3
Analytical expressions for the compression and shear stiffness and strength of pyramidal lattice truss sandwich structures [9,10]

Mechanical property	Analytical expression
Compressive stiffness	$E_c = E_s \cdot \sin^4\omega \cdot \eta \cdot \bar{\rho}$
Normalized compressive stiffness	$\Pi = \frac{E_c}{E_s \cdot \bar{\rho}} = \sin^4\omega \cdot \eta = 0.191$
Compressive strength (plastic yielding)	$\sigma_{pk} = \sigma_{ys} \cdot \sin^2\omega \cdot \eta \cdot \bar{\rho}$
Normalized compressive strength	$\Sigma = \frac{\sigma_{pk}}{\sigma_{ys} \cdot \bar{\rho}} = \sin^2\omega \cdot \eta = 0.382$
Compressive strength (elastic buckling)	$\sigma_{pk} = \sigma_{cr} \cdot \sin^2\omega \cdot \eta \cdot \bar{\rho}$, where $\sigma_{cr} = \frac{k^2\pi^2 E_s}{12}(\frac{t}{l})^2$
Compressive strength (plastic buckling)	$\sigma_{pk} = \sigma_{cr} \cdot \sin^2\omega \cdot \eta \cdot \bar{\rho}$, where $\sigma_{cr} = \frac{k^2\pi^2 E_t}{12}(\frac{t}{l})^2$
Shear stiffness	$G_c = \frac{1}{8}E_s \cdot \sin^2 2\omega \cdot \eta \cdot \bar{\rho}$
Normalized shear stiffness	$\Gamma = \frac{G_c}{E_s \cdot \bar{\rho}} = \frac{1}{8}\sin^2 2\omega \cdot \eta = 0.095$
Shear strength (plastic yielding)	$\tau_{pk} = \frac{1}{2\sqrt{2}}\sigma_{ys} \cdot \sin 2\omega \cdot \eta \cdot \bar{\rho}$
Normalized shear strength (plastic yielding)	$T = \frac{\tau_{pk}}{\sigma_{ys} \cdot \bar{\rho}} = \frac{1}{2\sqrt{2}} \cdot \sin 2\omega \cdot \eta = 0.270$
Shear strength (elastic buckling)	$\tau_{pk} = \frac{1}{2\sqrt{2}}\sigma_{cr} \sin 2\omega \cdot \eta \cdot \bar{\rho}$, where $\sigma_{cr} = \frac{k^2\pi^2 E_s}{12}(\frac{t}{l})^2$
Shear strength (plastic buckling)	$\tau_{pk} = \frac{1}{2\sqrt{2}}\sigma_{cr} \sin 2\omega \cdot \eta \cdot \bar{\rho}$, where $\sigma_{cr} = \frac{k^2\pi^2 E_t}{12}(\frac{t}{l})^2$

For the structures here, $\omega = 45°$ and $\eta = 0.763$.

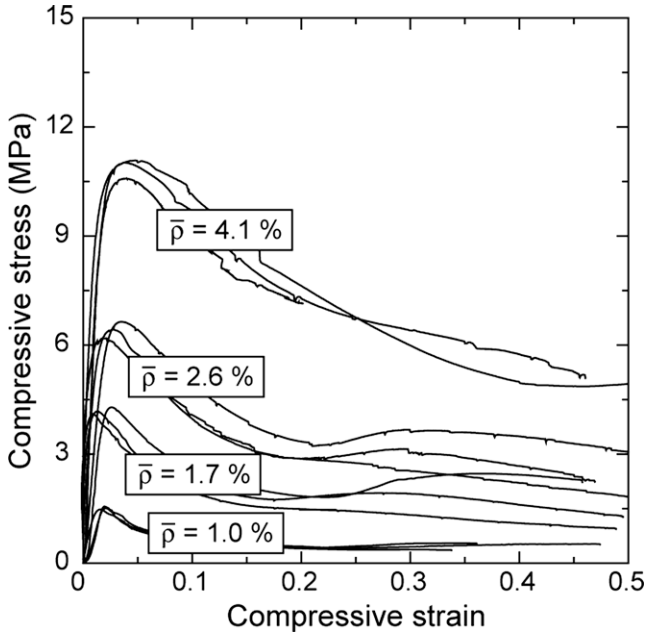

Fig. 6. Through thickness compressive stress–strain responses for Ti–6Al–4V lattice truss structures with relative densities, $\bar{\rho}$, between 1.0% and 4.1%.

ing an initial linear response, gradual core yielding was observed followed by a peak in the compressive stress. The lattice truss members within the structure plastically buckled shortly after yielding (at a strain of between 2% and 4%). Continued loading resulted in core softening followed by a stress plateau. The plateau stress of the structure corresponded to ~50% of the cores peak strength. Softening was coincident with buckling and the formation of a plastic hinge near the center of the truss member. Neither node nor truss fracture was observed during any of the compression experiments.

4.2. In-plane shear response

The longitudinal shear stress–strain responses are shown in Fig. 7. In the in-plane shear orientation, each unit cell has two truss members loaded in compression and two in tension. For some samples the shear stress–strain response exhibited a reasonably linear behavior followed by premature failure prior to the onset of an expected peak load, Fig. 7. This has been attributed to failure of the trusses and the truss–node interface. However, two of the $\bar{\rho} = 4.1\%$ cores did not fail prematurely and exhibited characteristics typical of lattice truss based sandwich cores including: elastic behavior during initial loading, followed by macroscopic yielding of the core and continued load support until a peak stress was reached which corresponded to the buckling of the compressed truss members. At high strain the load carrying capacity of the lattice structure decreased consistent with node debonding and tensile failure at the truss member–node interface, as shown Fig. 8a. A longitudinal metallographic image of a typical truss core–face sheet cross-section is shown in Fig. 8b. It can be seen that some residual porosity existed at the node–facesheet interface as well as a sharp stress concentration at the confluence of the trusses, the flat node and the facesheet.

5. Discussion

5.1. Compression

All the lattices showed a similar crush response consisting of an approximately linear initial loading followed by a distinct yield attainment of a peak strength and progressive softening there after. The initial elastic compressive response of the lattice truss cores was not perfectly linear. This is appears to arise from small differences in the lengths of the lattice truss members which results in non-uniform load distribution. This was consistent with experimentally observations of aluminum lattice structures which substantially stiffen once the peak load is reached [20].

Approximate analytical expressions for the compressive stiffness and strength of the pyramidal lattice truss cores can be developed following Deshpande and Fleck [9] and are summarized by the equations listed in Table 3. The unloading modulus just prior to lattice yield has been measured and plotted in Fig. 9a as a non-dimensional compressive stiffness, $\Pi = E_c/(E_s\bar{\rho})$ against the lattice relative density, $\bar{\rho}$. The analytical prediction of the non-dimensional compressive stiffness has a value of 0.191 and most of the experimental data lie within ±20% of this value. The lowest normalized stiffness corresponds to the highest relative density and the knock-down is attributed to truss waviness as seen in Fig. 5c and d. Fig. 9b shows the non-dimensional compressive peak strength, $\Sigma = \sigma_{pk}/(\sigma_y\bar{\rho})$ again plotted against $\bar{\rho}$. The analytical prediction of the non-dimensional compressive peak strengths are also plotted for plastic yielding, and elastic and plastic buckling. For the elastic and plastic buckling cases it was assumed that the truss members were either built-in at the facesheets, whereupon $k = 2$, or pin-jointed for which $k = 1$. The factor k depends on the rotational stiffness of the plastic hinge at the nodes; $k = 1$ for a joint that can freely rotate while $k = 2$ for fixed-joints which cannot

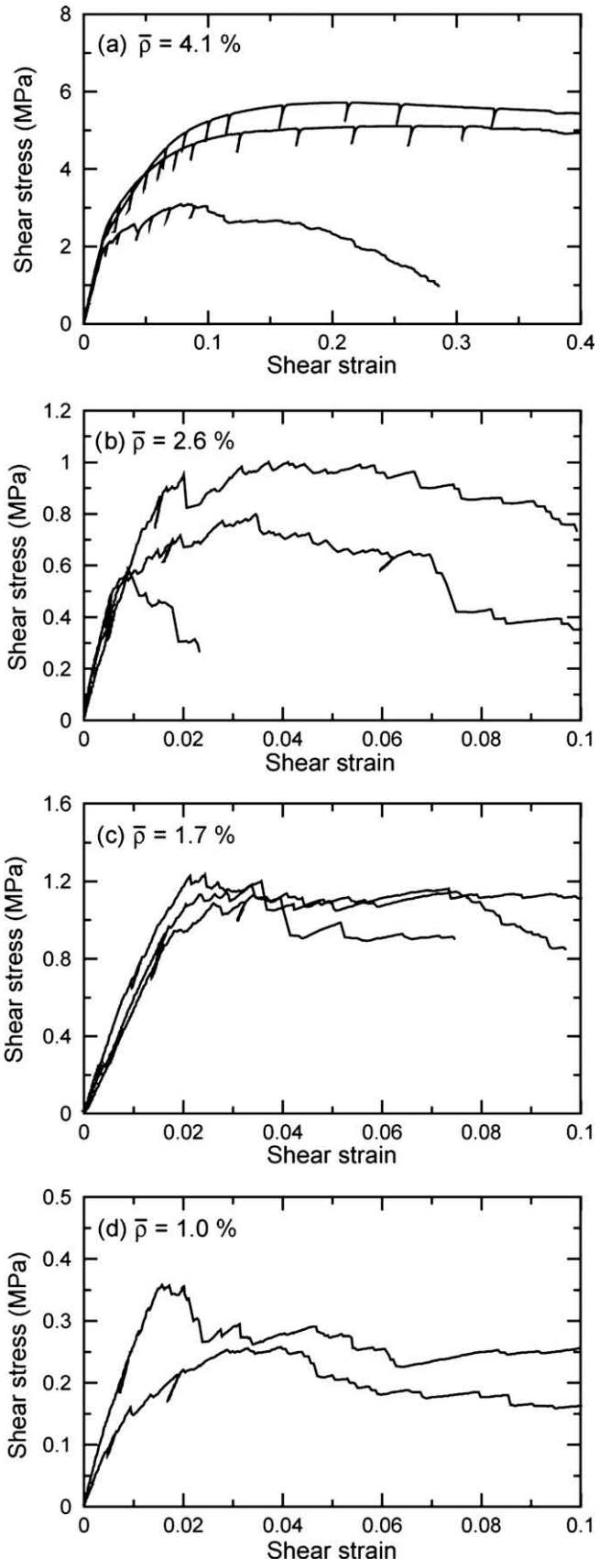

Fig. 7. Shear stress–strain responses for the Ti–6Al–4V lattice truss structures of different relative densities, $\bar{\rho}$.

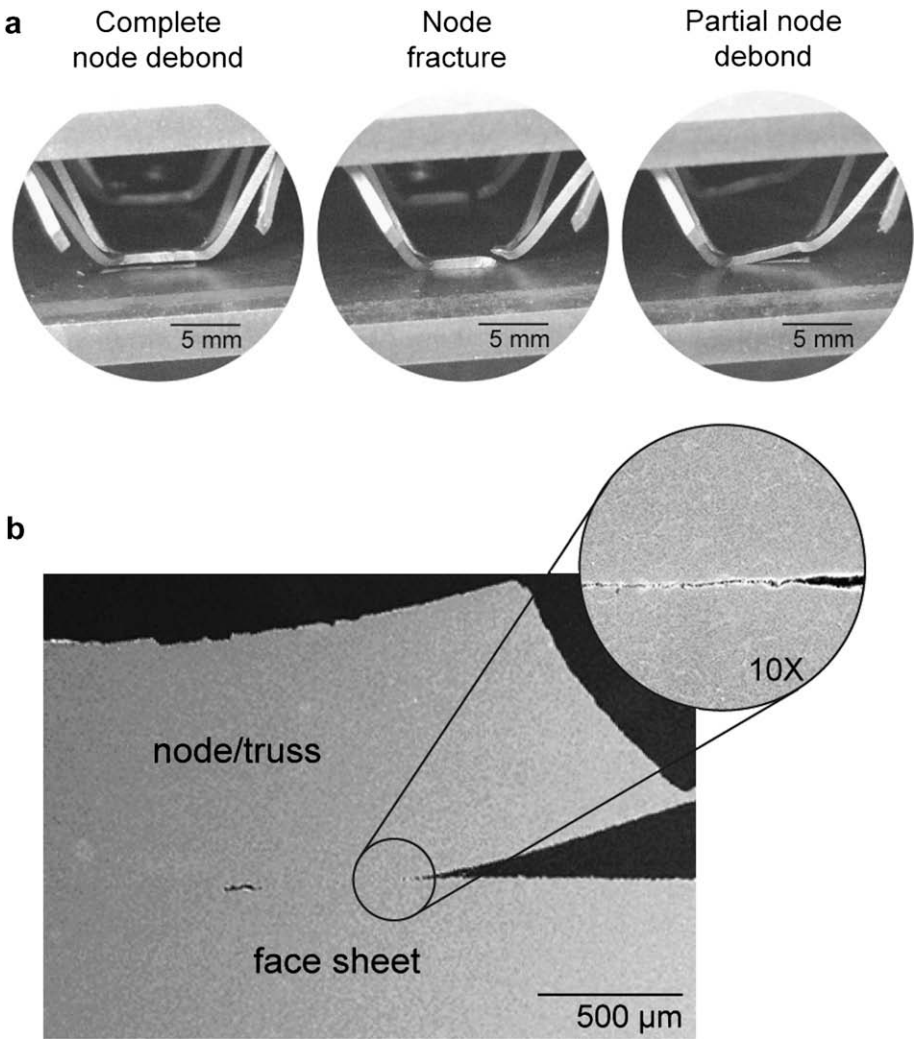

Fig. 8. (a) Photograph showing node debonding and fracture occurring during shear ($\bar{\rho} = 1.7\%$). (b) A longitudinal metallographic image of a representative diffusion bonded node–face sheet cross-section.

rotate. Fig. 9b shows that the plastic buckling model captures the strength dependence upon relative density for samples between 1.0% and 4.1%. For the lower density samples, the data are reasonably captured by the $k = 2$ approximation as minimal truss waviness was observed at the truss–facesheet interface. Whereas, truss waviness at the truss–facesheet confluence contributes towards the apparent decrease in strength coefficient for the higher relative density samples and the data lie closer to the $k = 1$ approximation.

5.2. Shear

Fig. 10a shows the non-dimensional shear stiffness, $\Gamma = G_c/(E_s\bar{\rho})$ plotted against $\bar{\rho}$. Again, approximate analytical expressions for the shear stiffness and strength of the pyramidal lattice truss cores have been developed and are summarized by the equations listed in Table 3. The predicted non-dimensional shear stiffness is also shown and it can be seen that the measured modulus is about half that predicted. This is thought to be a consequence of geometric imperfections in the trusses (truss waviness), core–facesheet misalignment and node debonding–truss tensile failure. The data reported here for the shear stiffness was taken at strains within the linear elastic region where geometric defects are most pronounced. Audible failures occurred at the onset of the shear tests and serrations in both the elastic and plastic regions of the stress–strain response were observed and correlated to fracture events and were accompanied by acoustic emissions [9,20]. These events also contribute to the low shear stiffness data.

The analytical predictions of the shear peak strengths are plotted in Fig. 10b. For the elastic and plastic buckling cases, it was assumed that the truss members were built-in at the facesheets ($k = 2$). In addition, a first-order model for panel failure by node flat shearing was developed for the modified pyramidal lattice structures. Maximum yield stress theory (assuming Tresca yield and plane stress conditions) predicts that the shear yield stress, $\tau_y = 0.5\sigma_y$, where σ_y is the uniaxial tensile yield stress [21,22]. This gives a $\tau_y = 450$ MPa for the node failure stress analysis of the modified pyramidal lattice. Assuming a node contact area of $b \cdot w$ per unit cell, the node flat shear fracture force that can be sustained is $\tau_y \cdot b \cdot w$ and the shear strength is calculated by dividing by the unit cell area and is also shown in Fig. 10b. This serves as an upper limit prediction assuming a perfect bond exists at the interface. Failure was also observed by shearing of the lattice struts of the pyramidal core at the joints with the facesheets. Again, assuming $\tau_y = 450$ MPa for the node shear-off stress analysis the node truss shear fracture strength dictated by the node cross-section area $t \cdot w$ and is also shown in Fig. 10b.

Several conclusions can be drawn from the data in Fig. 10b. For the geometry considered here, and for a relative density $\bar{\rho} < 10\%$,

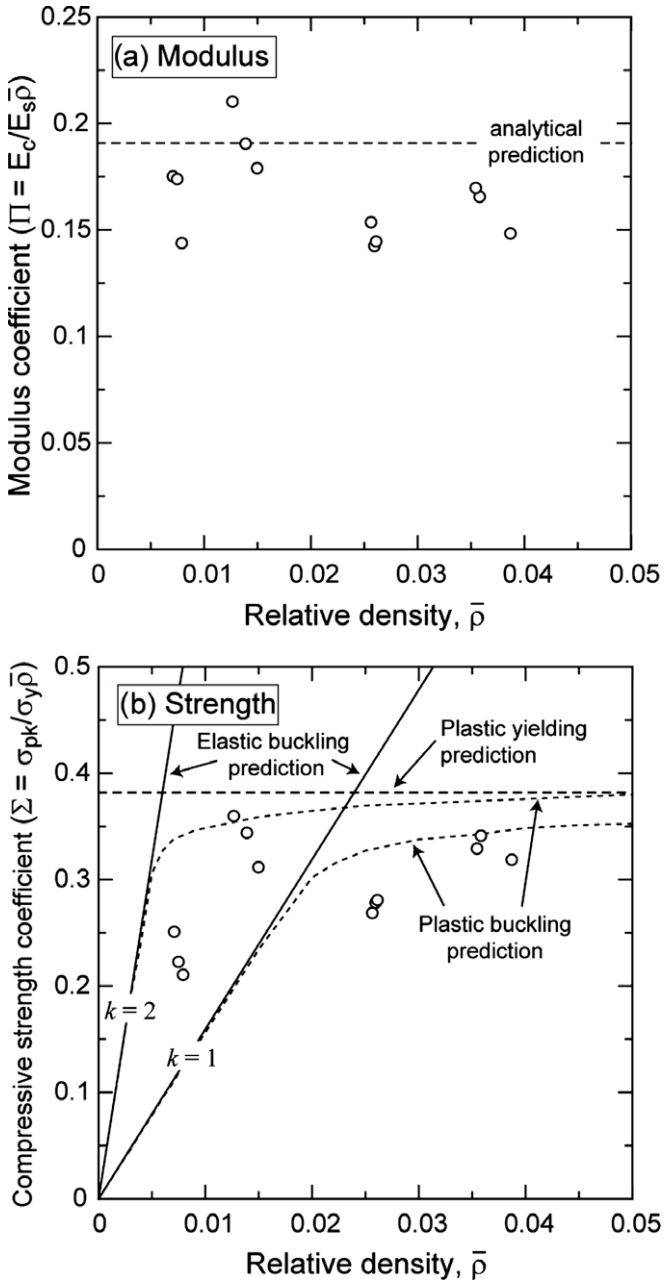

Fig. 9. Analytical predictions and experimental data for (a) compressive stiffness and (b) compressive strength coefficients.

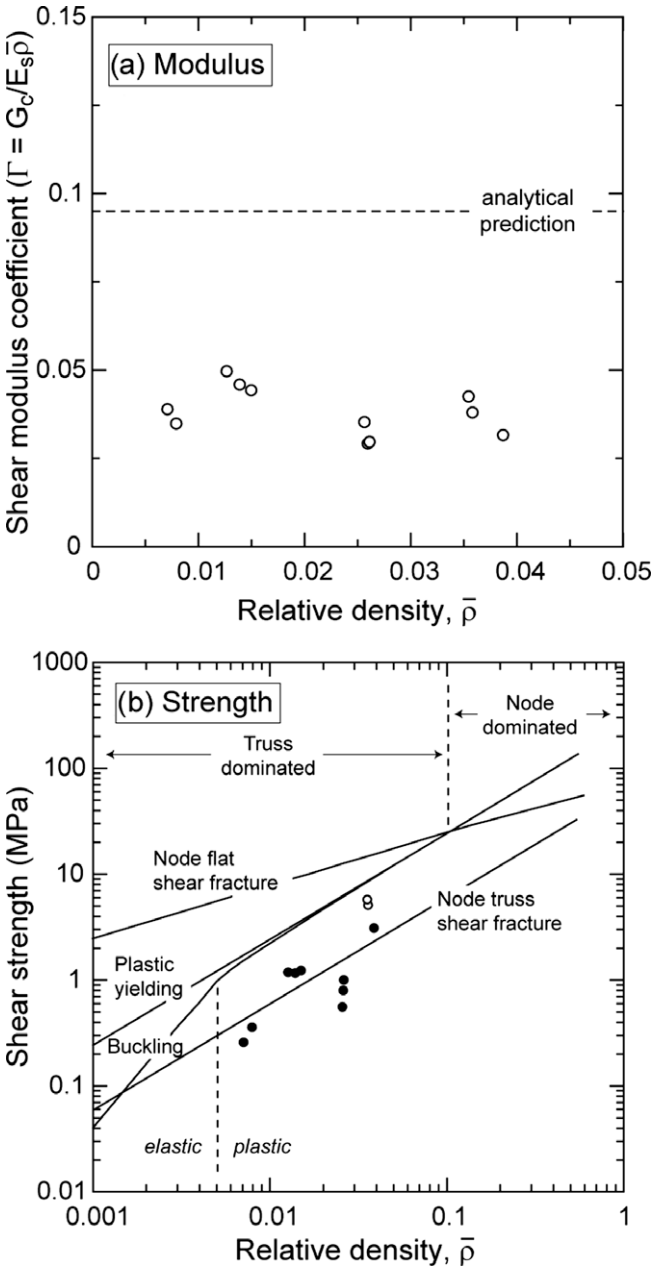

Fig. 10. Analytical predictions and experimental data for (a) the non-dimensional shear stiffness and (b) the shear strength as a function of relative density. Solid circles (●) indicate samples that failed at the nodes prior to the full peak strength.

panel failure in shear is predicted to be limited by either yielding by buckling (elastic or plastic) of the truss members assuming no node shear-off. As the relative density increases above 10%, failure is then limited by node flat shear fracture. However, for the geometry investigated here, node truss shear-off fracture dominates the behavior over a wide range of relative densities. The quality of the node joints between the core and the facesheet resulted in premature failure of a majority of the panels during shear loading by a combination of node flat shear fracture and node truss shear-off fracture and a majority of the data corresponds approximately with that predicted by node truss shear-off fracture.

5.3. Node–facesheet joint design issues

The design of the core to facesheet interface in honeycomb sandwich panels is of utmost importance. Ultimately, this dictates the amount of load which can be transferred from the facesheets to the core. As shown previously, this is similarly true for lattice based cores. Node bond failure has been identified as a key catastrophic failure mode for sandwich structures, especially titanium based honeycombs [23]. Similar node robustness issues have been previously observed during shear loading of lattice truss topologies [9,10,20]. When sandwich panels are subjected to shear or bending loads, the node transfers forces from the facesheets to the core members (assuming adequate node bond strength exists) and the topology for a given core relative density dictates the load carrying capacity. When the node–facesheet interface strength is compromised, from either poor joint design or bonding methods, node bond failure occurs and catastrophic failure of the sandwich panel results.

Titanium alloy honeycomb sandwich panels have been widely used in aerospace structures. They can be formed by either an expansion or corrugation processes [4,6]. Numerous methods have been proposed for joining titanium honeycomb cores to facesheets including: solid-state diffusion bonding [24–27], electron beam welding [28], and transient liquid interface diffusion bonding [29–35]. Solid-state diffusion bonding of titanium honeycomb structures is limited because stress-reducing fillets are not formed at the core–facesheet interface. During brazing, liquid interface diffusion and activated diffusion bonding processes, a liquid filler metal is drawn into the nodes and forms a stress-reducing fillet at the core–facesheet interface.

One potential mitigation strategy is to use a combination of hot forming/diffusion bonding, followed by brazing. Fig. 11a and b show longitudinal and transverse micrographs of a node/facesheet interface that has been hot formed/diffusion bonded by the process developed here and subsequently brazed. A Ticuni® braze alloy with a nominal composition of 60.0Ti–25.0Ni–15.0Cu wt.% was used as the braze alloy. The sample was vacuum brazed ($\sim 10^{-4}$ Torr chamber pressure) at a heating rate of 10 °C/min to 550 °C, held for 1 h (to volatilize the binder), then heated to the brazing temperature of 950 °C for 60 min prior to furnace cooling at ~25 °C/min. During brazing the molten alloy is drawn into the node–facesheet interface. It is seen in Fig. 11, that the combination of hot forming/diffusion bonding followed by brazing forms a large filet at the truss–facesheet interface. The presence of this filet reduces the stress concentration and increases the node contact area which is likely to reduce the local stress supported at the interface.

5.4. Comparisons with other topologies

To assess how well the Ti–6Al–4V modified pyramidal lattice trusses compete with other lattice and prismatic topologies in compression, the compressive peak strength, σ_{pk}, versus absolute density, ρ_s, is shown in Fig. 12. It can be seen from Fig. 12 that all the lattice and prismatic topologies roughly follow the same dependency upon density with the lattices out performing the prismatic topologies. In addition to the topology dependence, the parent materials strength-to-weight ratio affect becomes apparent. Ti–6Al–4V possesses a higher strength-to-weight ratio than 6061 aluminum and 304 stainless steel and therefore sandwich structures made from it are stronger on a per weight basis. In addition, increasing the truss mass fraction η from 0.76 to 1.0 would increase the specific strength of the Ti–6Al–4V lattice truss sandwich structures shown in Fig. 12 by ~25%.

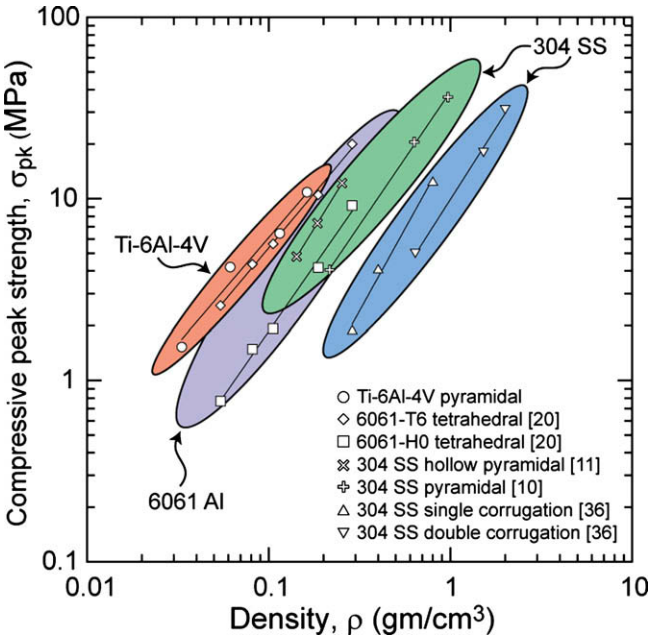

Fig. 12. Compressive peak strength versus density for various sandwich core topologies. (See above mentioned references for further information.)

6. Summary

- A new method for fabricating a pyramidal lattice truss structure has been developed using a combination of ambient temperature forming and a combination of high-temperature forming/diffusion bonding. The approach was illustrated by fabricating and testing sandwich panels using a Ti–6Al–4V alloy and appears extendable to other alloy systems that exhibit limited ambient temperature formability and are suitable for diffusion bonding.
- Analytical predictions for a regular pyramidal lattice truss structure have been adapted for modified lattices fabricated here. The stiffness and peak strength of these modified pyramidal lattices depends on three dominant factors: (i) the stress–strain response of the parent alloy, (ii) the truss mass fraction, η, and (iii) the relative density, $\bar{\rho}$, of the lattice core. The modified pyramidal lattices stiffness and strengths were shown to be reduced from that of an ideal pyramidal lattice by the truss mass efficiency factor η.

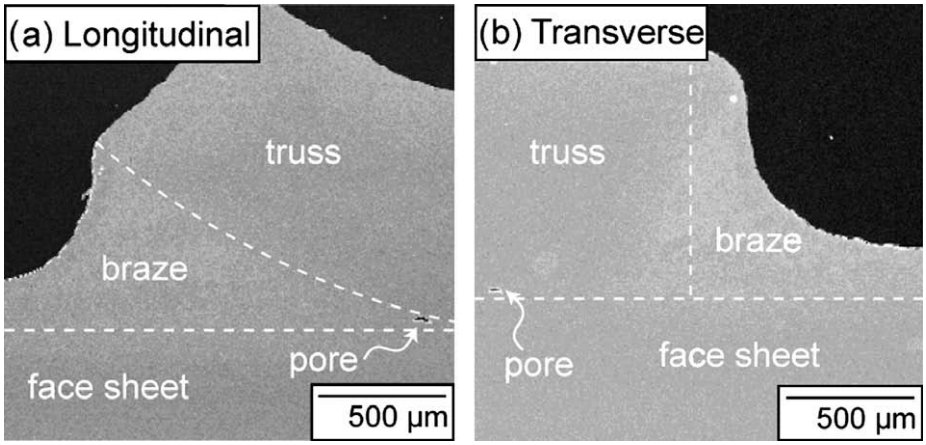

Fig. 11. Longitudinal and transverse metallographic images of a typical node–face sheet cross-section after diffusion bonding and subsequent brazing.

- During compressive and shear loading, the stress–strain responses were similar to other lattice truss based materials and the peak strengths corresponded to the onset of truss member buckling. The measured non-dimensional stiffness and strength coefficients were found to be in reasonable agreement with the analytical predictions.
- It was determined that for the current design, the predicted node contact area was sufficient to resist node flat shear failure during compressive deformation, but extensive node debonding and truss fracture occurred during shear deformation prior to the onset of the lattice cores peak load.
- A potential mitigation strategy has been proposed to increase the node fracture strength and a full optimization of the node bonding process and node interface geometry is forthcoming.

Acknowledgements

This work was supported by the Office of Naval Research (ONR), monitored by Drs. Steve Fishman and David Shifler under Grant No. N00014-01-1-1051. The authors would also like to thank Ken Ervin for his work on the early development of this fabrication methodology.

References

[1] Evans AG, Hutchinson JW, Ashby MF. Cellular metals. Curr Opin Solid State Mater Sci 1998;3:288–303.
[2] Evans AG, Hutchinson JW, Ashby MF. Multifunctionality of cellular metal systems. Prog Mater Sci 1999;43:171–221.
[3] Evans AG, Hutchinson JW, Fleck NA, Ashby MF, Wadley HNG. The topological design of multifunctional cellular metals. Prog Mater Sci 2001;46:309–27.
[4] Wadley HNG, Fleck NA, Evans AG. Fabrication and structural performance of periodic cellular metal sandwich structures. Compos Sci Technol 2003;63:2331–43.
[5] Wadley HNG. Multifunctional periodic cellular metals. Philos Trans Roy Soc A 2006;364:31–68.
[6] Bitzer T. Honeycomb Technology: materials, design, manufacturing, applications and testing. The Netherlands: Chapman & Hall; 1997.
[7] Allen HG. Analysis and design of structural sandwich panels. Oxford: Pergamon Press; 1969.
[8] Gibson LJ, Ashby MF. Cellular solids: structure and properties. 2nd ed. Cambridge: Cambridge University Press; 1997.
[9] Deshpande VS, Fleck NA. Collapse of truss core sandwich beams in 3-point bending. Int J Solids Struct 2001;38:6275–305.
[10] Zok FW, Waltner SA, Wei Z, Rathbun HJ, McMeeking RM, Evans AG. A protocol for characterizing the structural performance of metallic sandwich panels: application to pyramidal truss cores. Int J Solids Struct 2004;41:6249–71.
[11] Queheillalt DT, Wadley HNG. Pyramidal lattice truss structures with hollow trusses. Mater Sci Eng A 2005;397:132–7.
[12] Kooistra GW, Wadley HNG. Lattice truss structures from expanded metal sheets. Mater Des 2007;28:507–14.
[13] Biaggi R, Bart-Smith H. Imperfection sensitivity of pyramidal core sandwich structures. Int J Solids Struct 2007;44:4690–706.
[14] Queheillalt DT, Wadley HNG, The compressive and shear responses of hollow pyramidal lattice materials. J Mech Mater Struct, 2008, submitted for publication.
[15] Hosford WF, Caddell RM. Metal forming: mechanics and metallurgy. New Jersey: Prentice-Hall; 1983.
[16] Lascoe OD. Handbook of fabrication processes. Metals Park: ASM International; 1988.
[17] Yang CT. Calculating minimum bend radii from ductility ratings. Met Prog 1970;98:107–10.
[18] ASM metals handbook. vol. 1, Properties and selection: irons, steels, and high-performance alloys. 10th ed. Metals Park: ASM International; 1991.
[19] ASM metals handbook. vol. 2, Properties and selection: nonferrous alloys and special-purpose materials. 10th ed. Metals Park: ASM International; 1991.
[20] Kooistra GW. Lattice truss structures made from age hardenable aluminum alloys. Masters thesis, Department of Materials Science and Engineering, University of Virginia, 2005.
[21] Shanley FR. Mechanics of materials. New York: McGraw-Hill; 1967.
[22] Gere JM, Timoshenko SP. Mechanics of materials. Boston: PWS Engineering; 1984.
[23] Richards WL, Thompson RC. Titanium honeycomb panel testing. NASA Technical Memorandum, 1996. p. 4768.
[24] Kolom AL. Titanium diffusion-bonded honeycomb. Optimum structure for material, joining medium, and configuration. J Aircraft 1969;6:410–5.
[25] Emero DH, Mejia MJ. Metallurgical and structural aspects of diffusion bonded titanium honeycomb sandwich. SAMPE J 1970;6:11–7.
[26] Peshkov VV. Technological parameter of the process of diffusion bonding honeycomb structures made of titanium alloys. Weld Prod 1984;32:24–7.
[27] Bulkov AB, Peshkov VV, Batishchev AA, Bashkatov AV, Petrenko VR. Optimization of the microstructure of filler for titanium diffusion-welded thin-wall laminated structures. Weld Int 2005;19:148–51.
[28] Yanchuk LM, Smetanko VG, Shlyaev YuN. The electron-beam welding of titanium honeycomb structures. Weld Prod 1979;26:45–7.
[29] Woodward JR. Liquid interface diffusion method of bonding titanium and/or titanium alloy structure. US Patent 3,957,194, 1976.
[30] Woodward JR. Liquid interface diffusion method of bonding titanium and/or titanium alloy structure and product using nickel–copper, silver bridging material. US Patent 3,854,194, 1974.
[31] Woodward JR. Liquid interface diffusion method of bonding titanium and titanium alloy honeycomb sandwich panel structure. US Patent 3,769,101, 1973.
[32] Woodward JR. Liquid interface diffusion bonded titanium. US Patent 3,768,985, 1973.
[33] Woodward JR. Titanium honeycomb sandwich fabrication process. Int J Numer Methods Eng 1973:423–7.
[34] Wood N. New diffusion bonding process makes stronger honeycomb structures. Assembly Eng 1974;17(4):44–6.
[35] Huang X, Richards NL. Activated diffusion brazing technology for manufacture of titanium honeycomb structures – a statistical study. Weld J 2004;83:73–81.
[36] Côté F, Deshpande VS, Fleck NA, Evans AG. The compressive and shear responses of corrugated and diamond lattice materials. Int J Solids Struct 2006;43:6220–42.